Article

Optimal Power Flow with Stochastic Solar Power Using Clustering-Based Multi-Objective Differential Evolution

Derong Lv [1], Guojiang Xiong [1,2,*], Xiaofan Fu [1], Yang Wu [3], Sheng Xu [3] and Hao Chen [4,*]

1 College of Electrical Engineering, Guizhou University, Guiyang 550025, China
2 Guizhou University Institute of Engineering Investigation & Design Co., Ltd., Guiyang 550025, China
3 Guizhou Electric Power Grid Dispatching and Control Center, Guiyang 550002, China
4 Fujian Provincial Key Laboratory of Intelligent Identification and Control of Complex Dynamic System, Quanzhou 362216, China
* Correspondence: gjxiongee@foxmail.com (G.X.); chenhao@fjirsm.ac.cn (H.C.)

Abstract: Optimal power flow is one of the fundamental optimal operation problems for power systems. With the increasing scale of solar energy integrated into power systems, the uncertainty of solar power brings intractable challenges to the power system operation. The multi-objective optimal power flow (MOOPF) considering the solar energy becomes a hotspot issue. In this study, a MOOPF model considering the uncertainty of solar power is proposed. Both scenarios of overestimation and underestimation of solar power are modeled and penalized in the form of operating cost. In order to solve this multi-objective optimization model effectively, this study proposes a clustering-based multi-objective differential evolution (CMODE) which is based on the main features: (1) extending DE into multi-objective algorithm, (2) introducing the feasible solution priority technique to deal with different constraints, and (3) combining the feasible solution priority technique and the merged hierarchical clustering method to determine the optimal Pareto frontier. The simulation outcomes on two cases based on the IEEE 57-bus system verify the reliability and superiority of CMODE over other peer methods in addressing the MOOPF.

Keywords: optimal power flow; uncertainty; differential evolution; hierarchical clustering; Pareto frontier

1. Introduction

Optimal power flow (OPF) is a typical operation problem of power systems. The traditional OPF usually focus on minimizing the overall operating cost of thermal power generators. However, thermal power generators release massive pollutants during operation. Therefore, emission reduction has become one of the most notable hotspot issues. Under this background, power systems need to minimize the emission of pollutants while operating economically, which is also the purpose of the studied multi-objective optimal power flow (MOOPF).

MOOPF is a highly nonconvex and nonlinear multi-objective problem, especially with the valve-point effects of thermal generators. Linear programming [1] and dynamic programming [2] are representative classical methods for addressing the problem, but they are vulnerable to the issue of stagnation when applied to complicated problems [3]. Furthermore, they generally need to transform multiple objectives into one, so they cannot handle all the objectives at the same time and provide a group of compromise solutions when solving multi-objective problems.

Intelligent methods, as the most favorite approach in recent years, can optimize multiple objectives simultaneously without transforming these objectives. Moreover, they do not impose any form of restriction on the problem. In order to solve the MOOPF, Pulluri et al. [4] raised the ability of different evolution through a combination of eigenvector and binomial crossovers and self-adaptive parameter strategy. El-Sattar et al. [5] proposed a multi-objective Jaya algorithm to deal with this issue. Chen et al. [6] introduced

nonlinearly-adjusted coefficient, adaptive-adjusted map factor and penalty function into pigeon-inspired algorithm and combined a sorting rule to solve the problem. Naderi et al. [7] combined fuzzy strategy, differential evolution and self-adaptive particle swarm optimization to address the problem. Reddy [8] employed a multi-objective differential evolution to enhance the solving reliability and efficiency for MOOPF. Abbasi et al. [9] integrated an effective initialization method and differential evolution into harmony search. Biswas et al. [10] combined the feasible solution technology with classical decomposition based multi-objective evolutionary algorithm to address this complex problem.

In solving practical complex multi-objective engineering problems such as the MOOPF, achieving the optimal Pareto frontier (PF) is one of the most difficult issues. In order to solve this issue, Xiong et al. [11] proposed an improved correction strategy by combining the slope and the crowding distance to obtain a better PF. Warid et al. [12] presented a quasi-oppositional Jaya and used an external elitist repository to produce a well-distributed PF. Shi et al. [13] combined some diversity maintaining strategies to obtain a smooth PF. Hua et al. [14] proposed a clustering-based environment selection to address the issue. Li et al. [15] adopted the reinforcement learning to guide the agents toward a better PF. Zhang et al. [16] raised a non-dominated improved multi-objective teaching-learning-based optimization by introducing an adaptive teaching factor and a non-dominated ranking method based on crowding distance to find the best PF.

Solar photovoltaic (PV) power can help power systems achieve the purpose of energy saving and emission reduction significantly [17–19]. Nevertheless, with the increasing scale of PV power, its stochastic output [20,21] brings many challenges to the operation of power systems. Moreover, this strong uncertainty also makes the MOOPF more complex and the optimal PF is harder to be searched. In order to achieve a good PF for a complex multi-objective problem, the clustering-based technique is a workable way. The clustering-based technique, such as partitioning-based clustering, grid-based clustering, model-based clustering and density-based clustering, can scan solutions and help them approach a better PF. However, these clustering techniques also have some weaknesses [14]. For instance, the model-based clustering is complex and takes a long time. The grid-based clustering cannot be employed independently. The partitioning-based clustering needs to set up the cluster centers in advance. The density-based clustering is more likely to choose the individuals in the crowded regions, but some individuals in the sparse regions may be better.

In contrast with the above clustering-based techniques, the merging hierarchical clustering-based technique [22] does not require assumptions about the distribution of individuals. It also does not require the number of clusters to be set in advance. Inspired by the potential of the merging hierarchical clustering-based technique, we propose a multi-objective optimization algorithm named CMODE by hybridizing it with differential evolution (DE) and apply the resultant CMODE to the MOOPF considering the uncertainty of PV power in this work. Firstly, we extend DE to adapt to the multi-objective problem. Secondly, to address the MOEED reliably, we adopt the feasible solution priority technique to process different constraints. Thirdly, we incorporate the merging hierarchical clustering-based technique and the feasible solution priority technique to select compromise solutions to acquire the optimal PF.

The main contributions of this study are concluded below:

(i) A MOOPF model with the PV power uncertainty is presented. A method based on overestimating and underestimating the PV power output is introduced to processing the uncertainty.

(ii) A multi-objective method named CMODE is developed to solve the MOOPF model. Some approaches including fuzzy decision technique, feasible solution priority technique and merging hierarchical clustering are integrated into CMODE to raise its solving performance.

(iii) In order to test the usefulness of CMODE, two cases based on the IEEE 57-bus system are conducted. Furthermore, three advanced methods are selected to compare with CMODE.

The rest structure can be summarized as below. Section 2 introduces the studied MOOPF and the calculation of stochastic PV power. Section 3 briefly reviews the DE and the merged hierarchical clustering. Section 4 provides the proposed CMODE. Section 5 gives the testing results and Section 6 summarizes the conclusions and future work.

2. Mathematical Model of the Studied MOOPF

MOOPF is a complex optimization problem, mainly by adjusting some control variables to minimize the optimization objectives of power system while satisfying the operating constraints [23]. The optimization objectives of the studied MOOPF can be described as below:

$$Minimize : Y(p,o) = [E(p,o), C(p,o)] \tag{1}$$

$$subject\ to \begin{cases} g(p,o) \leq 0 \\ h(p,o) = 0 \end{cases} \tag{2}$$

where p and o are the vectors of control and state variables, respectively; $Y(p,o)$ means the objective functions; $E(p,o)$ means the total emission; $C(p,o)$ means the total operating cost; $g(p,o)$ means the set of inequality constraints; $h(p,o)$ means the set of equality constraints.

The group of control variables is used to control the system power flow and it can be described as below:

$$p = \left\{ P_{G2}, P_{G3}, \ldots, P_{GN_G}, V_{G1}, V_{G2}, \ldots, V_{GN_G}, T_1, T_2, \ldots, T_{N_{tr}} \right\} \tag{3}$$

where P_{Gm} and V_{Gm} are the active power and voltage of generator on bus m, respectively; T_m is the tap of mth transformer; N_G and N_{tr} are the number of generators and tap-regulated transformers, respectively.

The group of state variables is used to define the system state and it can be described as below:

$$o = \left\{ P_{G1}, V_{LB1}, V_{LB2}, \ldots, V_{LBN_{LB}}, Q_{G1}, Q_{G2}, \ldots, Q_{GN_G}, S_{L1}, S_{L2}, \ldots, S_{LN_L} \right\} \tag{4}$$

where P_{G1} is the active power of generator at swing bus; V_{LBm} is the voltage of mth load bus; Q_{Gm} is the reactive power of generator on bus m; S_{Lm} is the line loading of mth branch; N_{LB} and N_L are the number of load buses and branches, respectively.

2.1. Inequality and Equality Limits

(1)   Generator limits

$$Q_{Gm}^{\min} \leq Q_{Gm} \leq Q_{Gm}^{\max} \tag{5}$$

$$V_{Gm}^{\min} \leq V_{Gm} \leq V_{Gm}^{\max} \tag{6}$$

$$P_{Gm}^{\min} \leq P_{Gm} \leq P_{Gm}^{\max} \tag{7}$$

where $Q_{Gm}^{\min}$ and $Q_{Gm}^{\max}$ are the upper and lower reactive power limit of the mth generator, respectively; $V_{Gm}^{\min}$ and $V_{Gm}^{\max}$ are the upper and lower voltage limit of the mth generator, respectively; $P_{Gm}^{\min}$ and $P_{Gm}^{\max}$ are the upper and lower active power limit of the mth generator, respectively.

(2)   Transformer limits

$$T_m^{\min} \leq T_m \leq T_m^{\max} \tag{8}$$

where $T_m^{\min}$ and $T_m^{\max}$ are the upper and lower limit of the mth transformer, respectively.

(3)   Operation limits

$$V_{Bm}^{\min} \leq V_{Bm} \leq V_{Bm}^{\max} \tag{9}$$

$$S_{Lm} \leq S_{Lm}^{\max} \tag{10}$$

where V_{Bm} is the voltage on bus m; $V_{Bm}^{\min}$ and $V_{Bm}^{\max}$ are the upper and lower voltage limit of the mth bus, respectively; $S_{Lm}^{\max}$ is the upper limit of the capacity of branch m.

(4)   Power balance limits

$$P_{Gm} = V_{Bm} \sum_{n=1}^{N_B} V_{Bn}[B_{mn} \sin(\delta_m - \delta_n) + G_{mn} \cos(\delta_m - \delta_n)] + P_{Lm} \tag{11}$$

$$Q_{Gm} = V_{Bm} \sum_{n=1}^{N_B} V_{Bn}[G_{mn} \cos(\delta_m - \delta_n) - B_{mn} \sin(\delta_m - \delta_n)] + Q_{Lm} \tag{12}$$

where δ_m is the voltage angle on bus m; B_{mn} and G_{mn} are the susceptance and conductance between buses m and n, respectively; N_B is the number of buses; P_{Lm} and Q_{Lm} are the active and reactive load demand on bus m, respectively.

2.2. Operating Cost of Stochastic PV Power
2.2.1. Power Model of PV Power Plants

The power output of a PV power plant P_V varies with the solar irradiance R_I, and the output power is calculated as below:

$$P_V(R_I) = P_S(R_I/R_{I.std}) \tag{13}$$

where $R_{I.std}$ is the stands for the solar irradiance under the normal condition; P_S is the rated power of PV power plant.

In addition, the solar irradiance generally obeys the Lognormal probability density function $F(R_I)$, as given below [24]:

$$F(R_I) = \exp\left[\frac{-(\ln(R_I) - \varphi)^2}{2\gamma^2}\right]/R_I\gamma\sqrt{2\pi} \tag{14}$$

where φ and γ are the mean and standard deviation in Lognormal probability density function, respectively.

The distribution of S_I obtained by running 12,000 Monte Carlo scenes under $\varphi = 5.2$ and $\gamma = 0.6$ is illustrated in Figure 1.
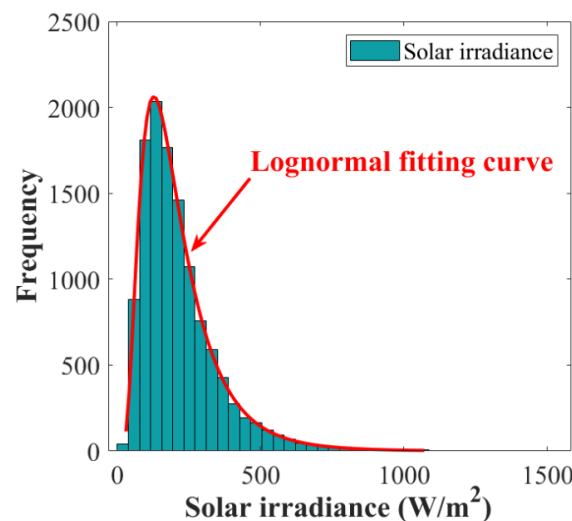

Figure 1. The distribution of solar irradiance.

2.2.2. Total Operating Cost of PV Power Plants

The output forecasting of a PV power plant has both possibilities of underestimation and overestimation [16]. Thus, in addition to the direct cost, the total operating cost also contains the cost for underestimation and overestimation scenarios.

The direct cost $C_{Vdm}(P_{Vm})$ is given by:

$$C_{Vdm}(P_{Vm}) = \varpi_d P_{Vm} \tag{15}$$

where P_{Vm} is the estimated power of mth PV power plant; ϖ_d is the direct cost factor.

The reserve cost $C_{Vrm}(P_{Vm})$ due to the underestimation is given by:

$$C_{Vrm}(P_{Vm}) = \varpi_r \sum_{n=1}^{N_{n-}} [(P_{Vm} - P_{n-})f_{n-}] \tag{16}$$

where ϖ_r is the reserve cost factor; P_{n-} is the active power lower than P_{Vm}; f_{n-} is the relative frequency of P_{n-}; N_{n-} is the number of P_{n-}.

The penalty cost $C_{Vpm}(P_{Vm})$ due to the overestimation is given by:

$$C_{Vpm}(P_{Vm}) = \varpi_p \sum_{n=1}^{N_{n+}} [(P_{n+} - P_{Vm})f_{n+}] \tag{17}$$

where ϖ_p is the penalty cost factor; P_{n+} is the active power higher than P_{Vm}; f_{n+} is the relative frequency of P_{n+}; N_{n+} is the number of P_{n+}.

Thus, the total cost C_V of N_V PV power plants is given by:

$$C_V = \sum_{m=1}^{N_V} \left(C_{Vdm}(P_{Vm}) + C_{Vrm}(P_{Vm}) + C_{Vpm}(P_{Vm}) \right) \tag{18}$$

2.3. Total Operating Cost of Thermal Generators

Thanks to the valve point effect, the operating curve of the thermal generator is highly nonlinear. The total operating cost C_T of N_T thermal generators is as below:

$$C_T = \sum_{m=1}^{N_T} \left\{ \eta_m P_m^2 + \mu_m P_m + \alpha_m + \left| l_m \times \sin\left[k_m \times \left(P_m - P_m^{\min} \right) \right] \right| \right\} \tag{19}$$

where P_m and $P_m^{\min}$ are the output and min power of mth thermal generator, respectively; η_m, μ_m and α_m are the operating cost factors of mth thermal generator; l_m and k_m are the valve-point effect factors of mth thermal generator.

2.4. Total Emission of Thermal Generators

The pollutant gases emitted by the thermal generators vary with their power outputs. The total emission E_T is as below:

$$E_T = \sum_{m=1}^{N_T} \left[e_m P_m^2 + d_m P_m + c_m + u_m \exp(g_m P_m) \right] \tag{20}$$

where e_m, d_m, c_m, u_m and g_m are the emission factors of mth thermal generator.

2.5. Optimization Objectives of the Studied MOOPF

The purpose of the studied MOOPF considering the PV uncertainty is to minimize both the overall emission and operating cost, which is as below:

$$Minimize : [E_T, C_T + C_V] \tag{21}$$

2.6. Operation Indicators

Two indicators including the total line power losses P_{loss} and voltage deviations V_D are employed to measure the operation quality.

$$P_{loss} = \sum_{L=1}^{N_L} G_{L(mn)} \left[V_{Bn}^2 - 2V_{Bn}V_{Bm}\cos(\delta_n - \delta_m) + V_{Bm}^2 \right] \tag{22}$$

$$V_D = \sum_{m=1}^{N_B} |1 - V_{Bm}| \tag{23}$$

where N_L is the number of branches; $G_{L(mn)}$ is the conductance of branch L connecting buses m and n.

3. Differential Evolution and Merged Hierarchical Clustering

3.1. Differential Evolution

DE is an advanced intelligent method that mainly contains four operators [25–28].

(1) Initialization. The optimization process starts from an initial population $Init\_pop$ with a set of individuals and each one is initialized as below:

$$x_{m,n}^0 = x_{m,n}^{min} + rand(0,1) \times (x_{m,n}^{max} - x_{m,n}^{min}) \tag{24}$$

where $m \in [1, N]$, N means the population size; $n \in [1, D]$, D means the problem scale; $rand(0,1)$ is a random value between 1 and 0; $x_{m,n}^{min}$ and $x_{m,n}^{max}$ mean the lower and upper limits, respectively.

Therefore, the initial population can be expressed as below:

$$Init\_pop = \left\{ x_1^G, x_2^G, \ldots, x_N^G \right\} \tag{25}$$

where G means the iteration counter.

(2) Mutation. It is to generate a mutant vector v_m^G from the target individual x_m^G by:

$$v_m^G = x_{r1}^G + F(x_{r2}^G - x_{r3}^G) \tag{26}$$

where F is the scaling factor; x_{r1}^G, x_{r2}^G and x_{r3}^G are three random distinct individuals.

(3) Crossover. Its intention is to combine x_m^G and v_m^G to produce a new vector u_m^G by:

$$u_{m,n}^G = \begin{cases} v_{m,n}^G, & \text{if } n = n_{rand} \text{ or } rand(0,1) \leq CR \\ x_{m,n}^G, & \text{otherwise} \end{cases} \tag{27}$$

where n_{rand} is a random integer within $[1, D]$; CR denotes the crossover rate.

(4) Selection. Its purpose is to select those superior individuals for the next iteration. Therefore, the more advantageous individual in x_m^G and u_m^G is retained, as shown below:

$$x_m^{G+1} = \begin{cases} u_m^G, & \text{if } Y(u_m^G) \leq Y(x_m^G) \\ x_m^G, & \text{otherwise} \end{cases} \tag{28}$$

where $Y(\cdot)$ means the fitness value.

3.2. Merged Hierarchical Clustering

In the merged hierarchical clustering, all points in a search space are treated as clusters [22]. These clusters are merged consecutively by a specific conjunction standard until they are grouped to one or the number of clusters reaches the predetermined value. The dendrogram of the merged hierarchical clustering is shown in Figure 2. The line between two different points means that they are merged into a new cluster by a special linkage. In order to divide the solutions as evenly as possible into the desired number of groups,

we use the Ward's linkage [29] as the conjunction criterion. The Ward's linkage maximizes the distance index $\tau(m, n)$ between different clusters, and minimizes the $\tau(m, n)$ within the same cluster. The calculation of the $\tau(m, n)$ is as below:

$$\tau(m, n) = \|\overline{U}_m - \overline{U}_n\|_2 \sqrt{2N_{Um}N_{Un}/(N_{Um} + N_{Un})} \tag{29}$$

where $\|\cdot\|_2$ means Euclidean distance; $\overline{U}_m$ and $\overline{U}_n$ mean the centers of the cluster m and the cluster n, respectively; N_{Um} and N_{Un} mean the total numbers of points in the clusters m and n, respectively.
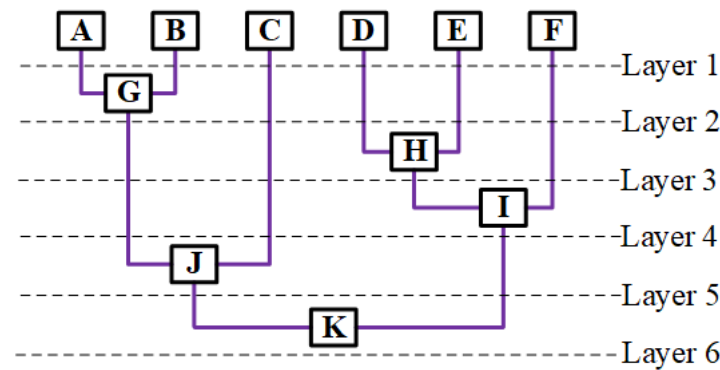
Figure 2. The dendrogram of the merged hierarchical clustering.

Here, we employ a bi-objective optimization problem to illustrate. Firstly, all points are treated as a single cluster and the $\tau(m, n)$ between every two points is calculated. Secondly, two points that have the smallest $\tau(m, n)$ are selected to merge into a new cluster. For instance, suppose $\tau(A, B)$ is the smallest, then A and B will be assigned into a new cluster G and the new cluster center is as below:

$$\overline{U}_g = \left(\frac{\sum_m^{N_{Ug}} Y_1^*(x_m)}{N_{Ug}}, \frac{\sum_m^{N_{Ug}} Y_2^*(x_m)}{N_{Ug}} \right) \tag{30}$$

For robust clustering, all objective values need to be normalized, as given below:

$$Y_j^*(x_m) = \left(Y_j(x_m) - Y_j^{\min} \right) / \left(Y_j^{\max} - Y_j^{\min} \right) \tag{31}$$

where $Y_j^*(\cdot)$ means the jth normalized objective value; $Y_j^{\max}$ and $Y_j^{\min}$ are the maximum and minimum values of the jth objective value.

This process will repeat until the terminal condition is met, i.e., the required number of the clusters is satisfied. As shown in Figure 1, different layers contain different clusters. For example, layer 1 contains five clusters, i.e., C, D, E, F and G, while layer 6 just contains one cluster K, so we can obtain the required number of clusters by setting the terminal condition.

4. Clustering-Based Multi-Objective Differential Evolution

4.1. Framework of CMODE

The flowchart of CMODE is shown in Figure 3. Firstly, a random population named Parent is first created and the fitness and the constraint violation values of each member in Parent are evaluated. Secondly, a population named Child is generated by crossing the target individuals and the mutant vectors. Next, the Parent and the Child are combined and the top N individuals are selected to become the new Parent. After that, the merged hierarchical clustering is performed on feasible solutions to achieve the PF. The above steps are executed until the stopping condition is met.

```
Initialize the random          Evaluate the fitness and all
     Population                 violation constraint values of each
                                      member in Parent

Input important                     Perform DE mutation
  information

     Start                    Generate the Child by crossing

                               Evaluate the fitness and all
 FEs = FEs + N                 violation constraint values of each
                                      member in Child

Combine Parent and Child , then sort
them  based on the violation constraint            End
value and sum of normalization of fitness

Select the top N                  Output the results
individuals to become the
    new Parent                         YES

 Is the no. feasible    NO        FEs > FESmax    NO
solutions at least N?

     YES              Perform merged
                   hierarchical clustering-
                   based determination of PF

                          gen = gen + 1
```

Figure 3. The flowchart of CMODE for the MOOPF problem.

4.2. Feasible Solution Priority Technique

In order to select the solutions that satisfy different constraints, we employ the feasible solution priority technique to address the problem. The technique uses a violation index $v(x)$ to judge the feasibility of solutions, as given below [30]:

$$v(x) = \sum_{w=1}^{N_W} \frac{I_w(x)}{I_w^{\max}} \Big/ \sum_{w=1}^{N_W} \frac{1}{I_w^{\max}} \qquad (32)$$

where N_W means the number of constraints; I_w means the violation of the wth constraint; $I_w^{\max}$ means the maximum value of I_w.

For two different solutions x_m and x_n, x_m is preferable to x_n according to the following criteria.

(1) Criterion 1: if $v(x_m) = 0$ and $v(x_n) \neq 0$.
(2) Criterion 2: if $v(x_m) = 0$, $v(x_n) = 0$, and $Y(x_m) \leq Y(x_n)$.
(3) Criterion 3: if $v(x_m) \neq 0$, $v(x_n) \neq 0$, and $Y(x_m) \leq Y(x_n)$.

4.3. Merged Hierarchical Clustering-Based Determination of PF

Since the number of feasible solutions may exceed the required value N, we propose to application of the merged hierarchical clustering to select superior solutions to form the PF, as shown in Algorithm 1.

We first combine the Parents of two adjacent generations to form a set U, and execute the fast non-dominated sort [31] on U to rank its members into different fronts. If the total

amount of members in U is equal to N, then all the members are selected to form the PF. Otherwise, if the total number members in U is higher than N, and the solutions in the first K fronts are less than N while the solutions in the first $(K + 1)$ fronts are higher than N, then we first retain all the solutions in the first K fronts in the PF. For the rest solutions, we make up them from the $(K + 1)$ front by using the merged hierarchical clustering.

In addition, to avoid the situation that some clusters contain no members while some clusters contain four or more members, we use the adjusting strategy in [14] to assign solutions to different clusters. In this way, the members in different clusters are distributed relatively evenly, which make the PF more uniform.

Algorithm 1: Merged hierarchical clustering-based determination of PF

Input: $(gen - 1)$th Parent and genth Parent
Output: PF
1: Combine the $(gen - 1)$th Parent and the genth Parent to for a set U.
2: Rank the solutions in U by executing the fast non-dominated sort
    % PF_K means the solutions in the first K fronts of U
    % $|PF_K|$ means the capacity of PF_K
3: **if** $|PF_K| = N$ **then**
4: PF = U, break
5: **else**
6: Select the rest R ($|R| = (N - |PF_K|)$) solutions from the $(K + 1)$ front of U with the merged hierarchical clustering
7: PF = $PF_K \cup R$
8: **end if**

4.4. The Determination of the Best Compromise Solution

The fuzzy decision technique is usually employed to extract the best compromise solution based on an index $\zeta(x_m)$ [25]:

$$\zeta(x_m) = \sum_{j=1}^{N_M} \zeta_j(x_m) / \sum_{m=1}^{N} \sum_{j=1}^{N_M} \zeta_j(x_m) \tag{33}$$

where N_M means the number of objectives.

The best compromise solution has the highest $\zeta(x_m)$. In Equation (32), the calculation of $\zeta_j(x_m)$ is as below:

$$\zeta_j(x_m) = \begin{cases} 1 & Y_j(x_m) \leq Y_j^{\min} \\ \frac{Y_j^{\max} - Y_j(x_m)}{Y_j^{\max} - Y_j^{\min}} & Y_j^{\min} \leq Y_j(x_m) \leq Y_j^{\max} \\ 0 & Y_j(x_m) \geq Y_j^{\max} \end{cases} \tag{34}$$

5. Simulation Results

5.1. Study Cases

CMODE is implemented to two different IEEE 57-bus systems and the systems' data are shown in Table 1. In the basic IEEE 57-bus system, seven thermal generators are connected to buses 1, 2, 3, 6, 8, 9 and 12 and bus 1 is the balancing node [32].

In order to study the effect of PV power plants on the system, we built a modified IEEE 57-bus system with three PV plants, as shown in Figure 4. In the modified IEEE 57-bus system, four thermal generators connected to buses 1, 3, 8 and 12 are retained, and the other three thermal generators connected to buses 2, 6 and 9 are replaced by three PV power plants. The parameters of these three PV power plants are presented in Table 2 and their available power is shown in Figure 5.

Table 1. The system information.

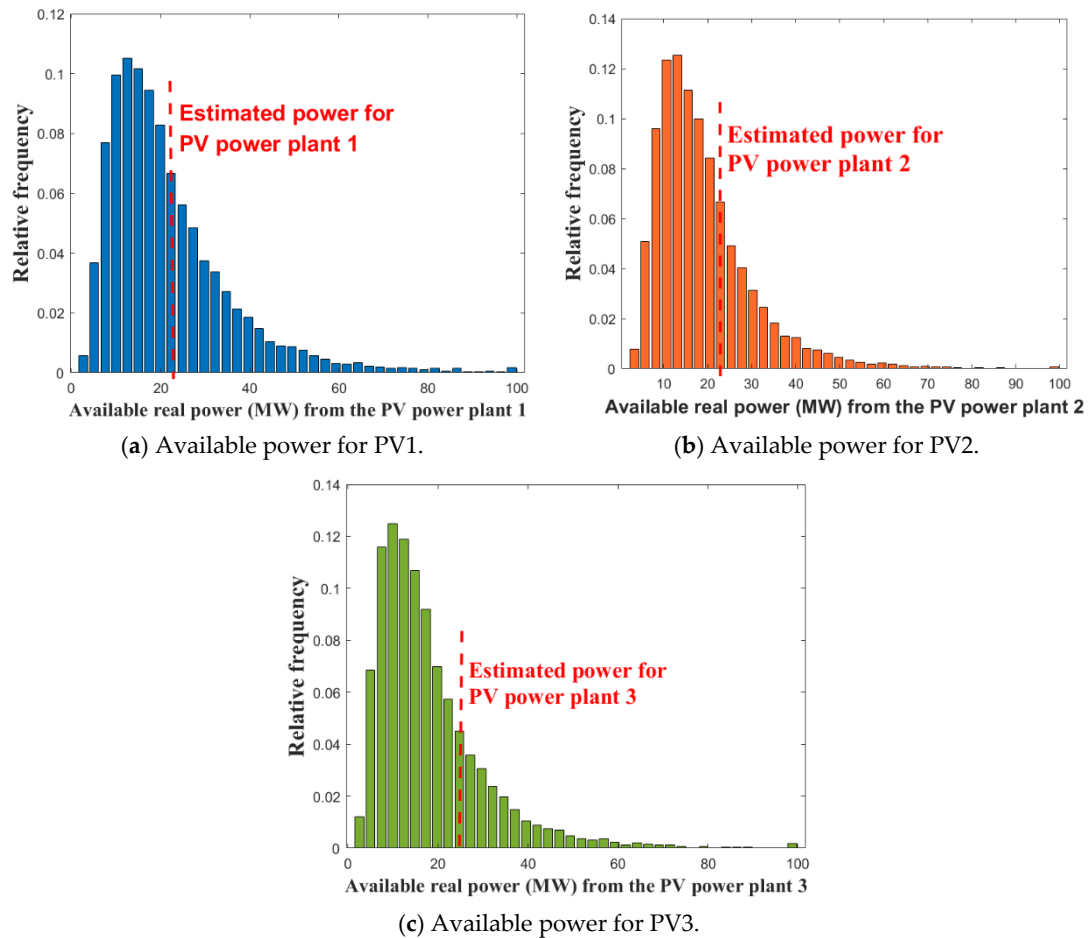| Items	Case1 IEEE 57-Bus System		Case2 Modified IEEE 57-Bus System	
	Quantity	Details	Quantity	Details
Buses	57	-	57	-
Branches	80	-	80	-
Thermal generators	7	Buses: 1 (Balancing Node), 2, 3, 6, 8, 9 and 12	4	Buses: 1 (Balancing Node), 3, 8 and 12
PV power plant	0	-	3	Buses: 2, 6 and 9
Transformer	17	Branches: 19, 20, 31, 35, 36, 37, 41, 46, 54, 58, 59, 65, 66, 71, 73, 76, 80	17	Branches: 19, 20, 31, 35, 36, 37, 41, 46, 54, 58, 59, 65, 66, 71, 73, 76, 80
System load	-	1250.8 MW, 336.4 MVAr	-	1250.8 MW, 336.4 MVAr
Load bus	50	Allowable voltage range: [0.94–1.06]	50	Allowable voltage range: [0.94–1.06]
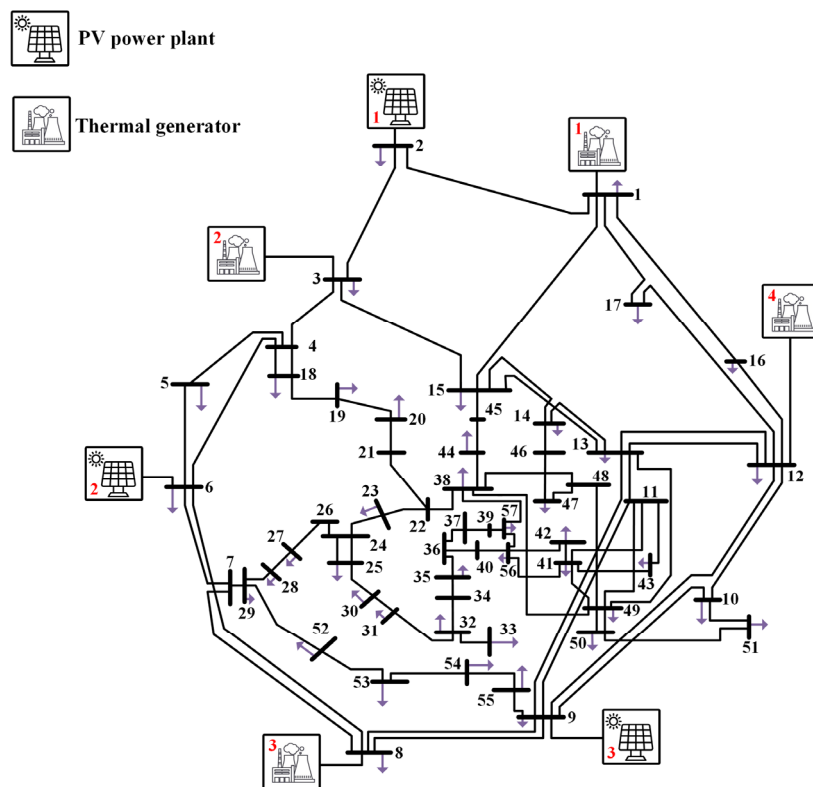
Figure 4. The wiring diagram of the modified IEEE 57-bus system (red 1 to 4—power sources, black 1 to 57—buses).

Table 2. The parameters of the three solar photovoltaic plants.

Plant	$R_{I.std}$ (W/m^2)	Rated Power (MW)	The Parameters in Probability Density Function	Cost Factors ($/MW)
PV1			$\varphi = 5.2$; $\gamma = 0.6$	
PV2	1000	100	$\varphi = 5.1$; $\gamma = 0.58$	$\varpi_d = 1.7$; $\varpi_r = 3.1$; $\varpi_p = 1.5$
PV3			$\varphi = 5$; $\gamma = 0.62$	

(**a**) Available power for PV1.

(**b**) Available power for PV2.

(**c**) Available power for PV3.

Figure 5. Available power of the three PV power plants.

5.2. Simulation Settings

Since the true optimal PF of the MOOPF is unavailable, the indicator Hypervolume (HV) is generally used to compare different algorithms. HV is described as below [33]:

$$HV(RP, PF) = \bigcup_{x \in PF}^{PF} \vartheta(RP, x) \tag{35}$$

where RP is the reference point $(1, 1)$; ϑ is the hypercube size enclosed by RP and x. This indicator can reflect an algorithm's convergence and diversity. The higher the HV, the better the performance.

In order to test the workability of CMODE in tackling the MOOPF problem considering the uncertainty of PV power, it is compared with three peer methods, i.e., NSGA-II [34], CA-MOEA [14] and GrEA [35]. Their parameters settings are listed in Table 3. To ensure the fairness, 30 independent trials were executed and the termination condition for each trial is $FEs_{max} = 4 \times 10^4$.

Table 3. Parameters settings of CMODE and other rivalries.

Method	Parameter Settings
CMODE	$N = 200$; $F_m^G = 0.1 + 0.9 \cdot rand$; $CR_m = rand$
NSGA-II	$N = 200$; mutation factor $P_M = 1/D$; crossover factor $P_C = 1$ crossover parameters $D_M = 20$, $D_C = 20$
CA-MOEA	$N = 200$; $P_C = 1$; $P_M = 1/D$; $D_M = 20$; $D_C = 20$
GrEA	$N = 200$; $P_C = 1$; $P_M = 1/D$; $D_M = 20$; $D_C = 20$; the number of divisions in each objective $DIV = 45$

5.3. Comparison of HV Results and Statistical Analysis

Table 4 shows, in both two cases the CMODE is the best one since its mean HV values are all higher than other methods. Although the standard deviation values of HV of CMODE are not the least.

Table 4. Comparison of HV results.

Algorithm	Case 1 Mean	Std.	Case 2 Mean	Std.
CMODE	0.07347	8.53×10^{-3}	0.08413	7.67×10^{-3}
NSGA-II	0.07241	5.99×10^{-3}	0.07176	5.34×10^{-3}
CA-MOEA	0.06316	6.03×10^{-3}	0.07912	5.00×10^{-3}
GrEA	0.07288	5.09×10^{-3}	0.07719	9.45×10^{-3}

Table 5 provides the outcomes of Wilcoxon's rank-sum test between CMODE and its rivalries at the 0.05 confidence level to reveal the statistical difference. The null hypothesis is that there is no significant difference between CMODE and the compared algorithms. The significance level is 0.05, and the hypothesis is rejected if the p-value is less than or equal to 0.05, i.e., there is a significant difference between the two algorithms compared. If the p-value is greater than 0.05, the hypothesis is accepted, i.e., there is no significant difference between CMODE and the compared algorithms. The signs "+" and "≈"represent that CMODE is signally superior or similar to its rivalries. Although MODE is statistically similar to NSGA-II and GrEA in case 1, the R^+ value is higher than the R^- value. In the case 2, CMODE is the best. Overall, the comparison indicates that CMODE outperforms its rivalries.

Table 5. R^-, p-value for the HV values of CMODE and other rivalries.

CMODE vs.	Case	R^+	R^-	p-Value	Sign
NSGA-II	Case 1	248	217	7.50×10^{-1}	≈
	Case 2	450	15	0.80×10^{-5}	+
CA-MOEA	Case 1	432	33	4.10×10^{-5}	+
	Case 2	373	92	3.85×10^{-3}	+
GrEA	Case 1	241	224	8.61×10^{-1}	≈
	Case 2	361	104	8.20×10^{-3}	+

5.4. Comparison of PF

We define the PF with the highest HV as the best PF, and conversely the PF with the lowest HV as the worst PF. The best and worst PF curves of all methods in these two cases are graphed in Figures 6 and 7, respectively. In Figure 6a, the points of GrEA are more dispersed than CMODE, indicating it has a better diversity, but its convergence is inferior to CMODE. In Figure 6b, GrEA and CA-MOEA have a rich diversity and the convergence of NSGA-II is poor, the diversity and convergence of CMODE are in the mid. In Figure 7a, the diversity of CMODE is the best. In Figure 7b, CMODE has a richer diversity and the convergence of GrEA is the worst.
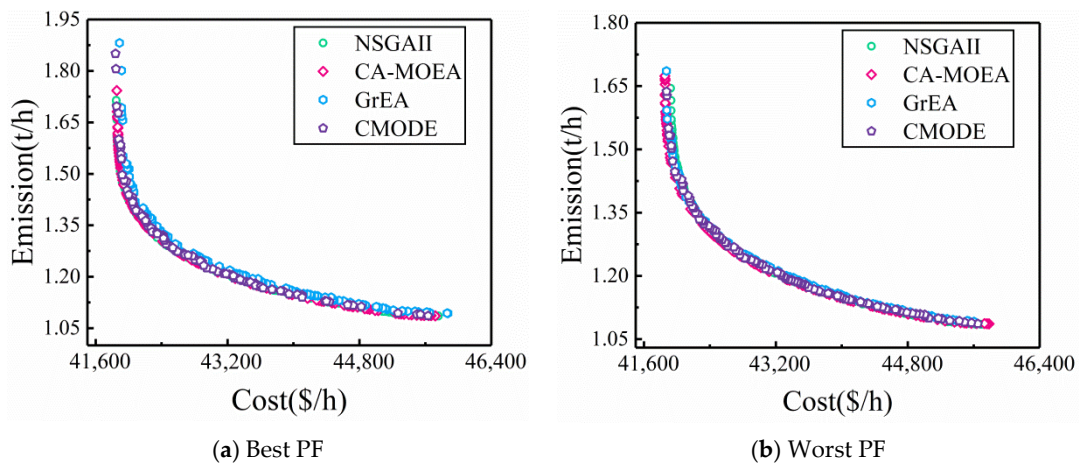
Figure 6. The comparison of the PFs of all methods in case 1.

Figure 7. The comparison of the PFs of all methods in case 2.

The difference between the best PF and the worst PF offered by CMODE is illustrated in Figure 8. In Figure 8a, the convergence in two scenarios is almost the same, but the best PF has a richer diversity signally. In Figure 8b, the diversity of the best PF is better than the worst signally.

Figure 8. The comparison of the best and the worst PFs of CMODE.

5.5. Comparison of Solutions
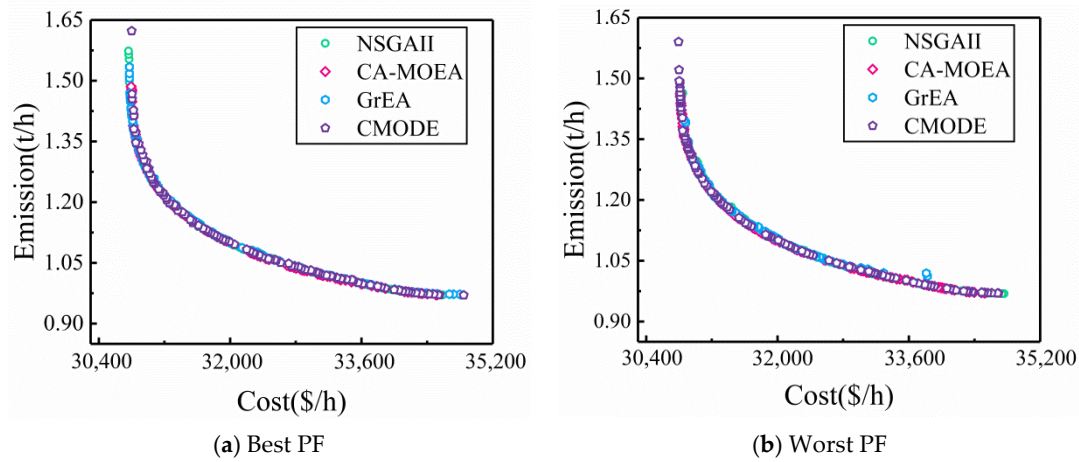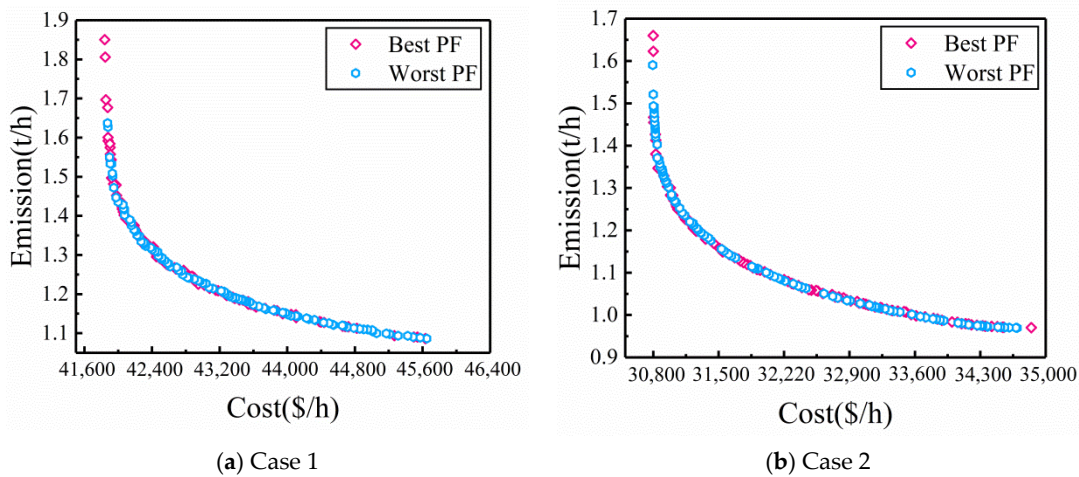
Tables 6 and 7 give the results of three scenarios including the best compromise solution, the best cost solution, and the best emission offered by all methods in these two cases, respectively. Table 6 shows that in the three scenarios, GrEA offers the minimum cost 41,810.32857 $/h and CMODE yields the minimum emission 1.08585 t/h. With regard to the best compromise solution, according to the operation indicators, NSGA-II acquires the best one and CMODE is slightly better than CA-MOEA and GrEA. Table 7 indicates that the minimum cost is 30,778.96877 $/h and the minimum emission is 0.97188 t/h, where both data are provided by CMODE. For the best compromise solution of COMDE, the power loss is 14.92952 MW and the voltage deviation is 0.97206 p.u., which are slightly better than GrEA. Overall, CMODE can provide highly competitive solutions in these two cases. Moreover, the detail solutions offered by CMODE are provided in Tables A1 and A2 in the appendix.

Table 6. The comparison of part of solutions in case 1.

Method	Situation	Cost ($/h)	Emission (t/h)	P_{loss} (MW)	V_D (p.u.)
CMODE	Best Comp	42,378.25740	1.29978	14.39902	1.08593
	Best Cost	41,829.54006	1.60733	15.44529	1.17172
	Best Emission	45,553.66027	1.08585	16.51269	1.13773
NSGA-II	Best Comp	42,514.14538	1.28064	14.29878	1.06271
	Best Cost	41,835.31986	1.70183	16.62134	1.05436
	Best Emission	45,562.55097	1.08711	17.78190	1.05475
CA-MOEA	Best Comp	42,300.31554	1.49821	14.64055	1.12854
	Best Cost	41,829.85245	1.73326	16.56421	1.15373
	Best Emission	46,741.88170	1.18792	19.42758	1.10973
GrEA	Best Comp	42,095.55055	1.39710	15.70217	1.19019
	Best Cost	41,810.32857	1.74843	16.72726	0.93812
	Best Emission	46,334.09802	1.09455	18.51497	0.92364

Table 7. The comparison of part of solutions in case 2.

Method	Situation	Cost ($/h)	Emission (t/h)	P_{loss} (MW)	V_D (p.u.)
CMODE	Best Comp	31,510.96410	1.15458	14.92952	0.97206
	Best Cost	30,778.96877	1.51445	16.06183	0.99820
	Best Emission	34,763.02046	0.97188	18.75483	0.93152
NSGA-II	Best Comp	31,878.11249	1.10791	14.73706	1.20800
	Best Cost	30,960.60974	1.32659	16.33062	1.28074
	Best Emission	34,584.57320	0.97317	17.36800	1.23202
CA-MOEA	Best Comp	31,363.89771	1.18054	14.38301	1.17212
	Best Cost	30,860.00681	1.43874	16.46837	1.11257
	Best Emission	34,804.96768	0.97553	17.17602	1.18253
GrEA	Best Comp	31,528.49233	1.16682	16.37542	1.15121
	Best Cost	30,858.11783	1.58188	19.11846	1.10638
	Best Emission	34,888.15443	0.97865	17.70621	1.02394

In order to further verify the reliability of the solutions, the bus voltages of all the three scenarios in these two cases are graphed in Figures 9 and 10, respectively. Figures 9a and 10a present the generator bus voltage plots, i.e., voltage control variables plots. Figures 9b and 10b present the load bus voltage plots, i.e., voltage state variables plots. In Figures 9 and 10, all the bus voltages are within the limits, further indicating the effectiveness of CMODE in achieving feasible solutions in different scenarios. In both two cases, the voltages of buses 18, 25, 29 and 51 are closer to the upper boundary, indicating that overvoltage may occur in these buses. This is mainly because these buses are closer to the power sources. On the other hand, the voltages of 20, 34 and 57 are closer to the lower boundary, indicating that insufficient reactive power may occur in these buses and the main reason is that these buses are far away from the power sources.
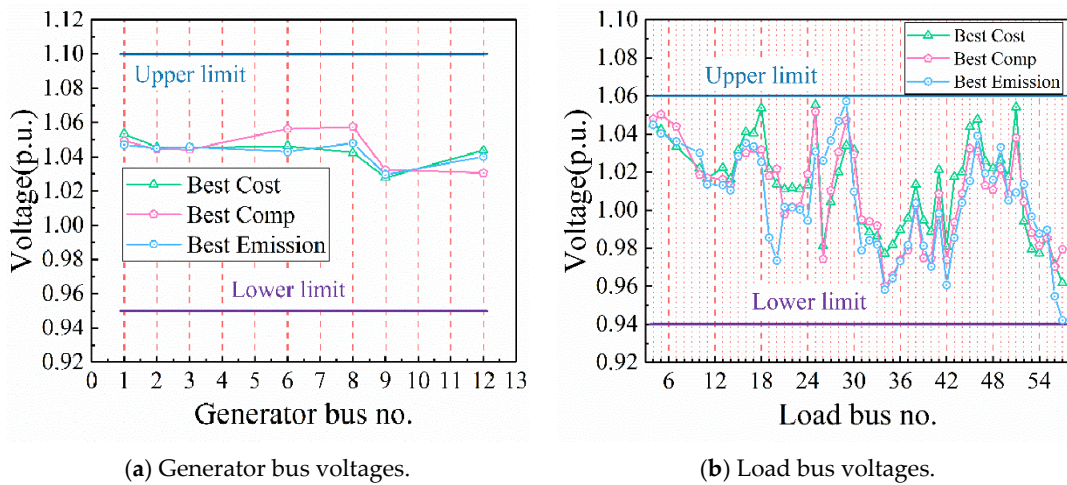
(**a**) Generator bus voltages.

(**b**) Load bus voltages.

Figure 9. The bus voltages in the three solution scenarios obtained by CMODE for case 1.

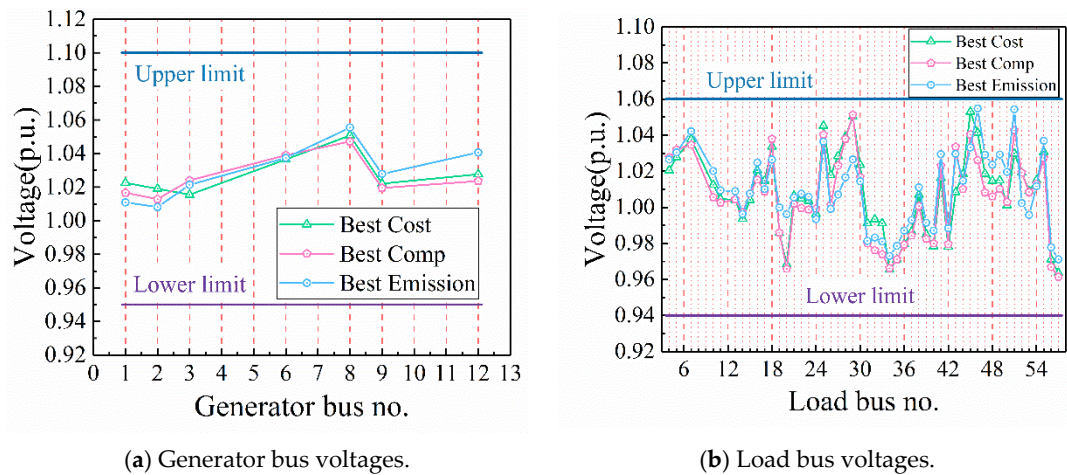(**a**) Generator bus voltages.

(**b**) Load bus voltages.

Figure 10. The bus voltages in the three solution scenarios obtained by CMODE for case 2.

In addition, the active power outputs (as shown in Figure 11a) of thermal generators and PV power plants and the corresponding emissions (as shown in Figure 11b) and operating costs (as shown in Figure 11c) provided by CMODE in the three scenarios for cases 1 and 2. Since the operating cost of PV power plants is relatively low and they do not emit polluting gases, so both the operating cost and emission in case 1 are consistently higher than those in case 2. To be specific, the introduction of PV power plants can reduce the total operating cost by 26.42% for the best cost solution scenario. On the other hand, the introduction of PV plants can also reduce the total emission by 10.50% for the best emission solution scenario. This is also the main reason for the massive use of solar energy. Tables 6 and 7 also indicate that the PV power can reduce the operating cost and emission significantly.
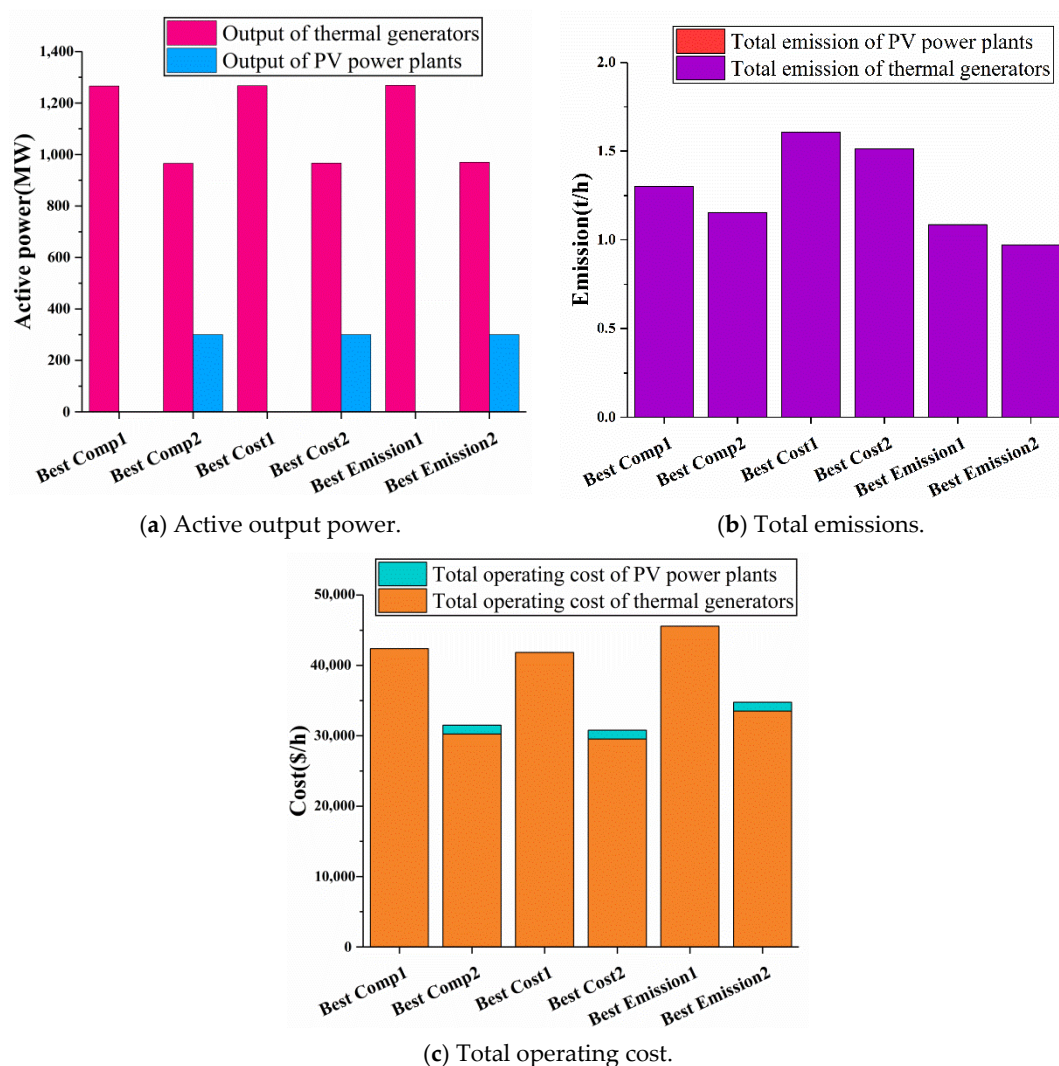
(**a**) Active output power.

(**b**) Total emissions.

(**c**) Total operating cost.

Figure 11. The active output power and total operating cost in the three scenarios (1-case 1, 2-case 2).

6. Conclusions and Future Work

A MOOPF model considering the solar uncertainty is constructed, and a method CMODE is developed to better address the MOOPF model. The effectiveness of CMODE is validated by comparing the simulation outcomes with other methods in two cases. According to the results of HV, it is clear that the PFs offered by CMODE are overall better. From the results of the best solutions of three scenarios in these two cases, CMODE also provides competitive feasible solutions. With the penetration of PV power plants in power system, the operating cost and the emission are reduced by 26.42% and 10.50%, respectively. Therefore, the solar PV power brings significant economic and environmental benefits.

In this work, only the PV power uncertainty is considered. In future work, we plan to consider the PV self-consumed electricity and use prediction methods to obtain a more accurate and effective PV power model. Furthermore, we intend to consider more uncertainties including wind and loads in the MOOPF model. Moreover, some techniques such as reinforcement learning and hybridization will be integrated to further boost CMODE.

Author Contributions: Conceptualization, D.L. and G.X.; methodology, D.L. and G.X.; formal analysis, G.X. and X.F.; resources, Y.W. and S.X.; writing—original draft preparation, D.L.; writing—review and editing, G.X. and X.F.; supervision, G.X.; funding acquisition, H.C. All authors have read and agreed to the published version of the manuscript.

Data Availability Statement: Not applicable.

Conflicts of Interest: The authors declare no conflict of interest.

Nomenclature

OPF	Optimal power flow
MOOPF	Multi-objective OPF
PF	Pareto frontier
PV	Photovoltaic
HV	Hypervolume
p, o	Control/state variables
$g(p, o), h(p, o)$	Inequality/equality constraints
Q_{Gm}, P_{Gm}, V_{Gm}	Reactive power/active power/voltage of generator bus
T_m	Tap setting of the mth transformer
V_{Bm}, δ_m	Voltage/voltage angle of bus
$P_{Gm}^{\min}, P_{Gm}^{\max}$	Upper/lower active power limit of the mth generator
$Q_{Gm}^{\min}, Q_{Gm}^{\max}$	Upper/lower reactive power limit of the mth generator
$V_{Gm}^{\min}, V_{Gm}^{\max}$	Upper/lower voltage limit of the mth generator bus
$V_{Bm}^{\min}, V_{Bm}^{\max}$	Upper/lower voltage limit of the mth load bus
S_{Lm}	Active power of the mth branch
$T_m^{\min}, T_m^{\max}$	Upper/lower tap limit of the mth transformer
$S_{Lm}^{\max}$	Upper limit of the capacity of the mth branch
B_{mn}, G_{mn}	Susceptance/conductance between buses m and n
P_{Lm}, Q_{Lm}	Active/reactive load demand on the mth bus
P_m	Output power of the mth generator
P_{Vm}, P_S	Estimated/rated power of the mth PV power plant
$R_{I.std}$	Solar irradiance under the normal condition
φ, γ	Mean/standard deviation of Lognormal probability density function
$\varpi_d, \varpi_r, \varpi_p$	Direct/reserve/penalty cost factor
P_{n-}, P_{n+}	Active power lower/higher than P_{Vm}
f_{n-}, f_{n+}	Relative frequency of P_{n-}/P_{n+}
N_{n-}, N_{n+}	The number of discrete pillars in P_{n-}/P_{n+}
$N_V, N_T, N_{LB}, N_B, N_L, N_{tr}$	The number of PV plants/thermal generators/load buses/buses/branches/tap-regulated transformers
l_m, k_m	Valve-point effect factors of the mth thermal generator
η_m, μ_m, α_m	Operating cost factors of the mth thermal generator
e_m, d_m, c_m, u_m, g_m	Emission factors of the mth thermal generator
P_{loss}, V_D	Total line power losses/voltage deviations

Appendix A

Table A1. Best solutions offered by CMODE in case 1.

Case 1		Min	Max	Best Comp	Best Cost	Best Emission
	P_{TG1} (MW)	0	575.88	186.3772	148.6171	223.4129
	P_{TG2} (MW)	30	100	100.0000	93.6162	100.0000
	P_{TG3} (MW)	42	140	70.8060	43.9203	140.0000
	P_{TG4} (MW)	30	100	99.8049	99.8664	100.0000
	P_{TG5} (MW)	165	550	364.2674	425.0176	287.8140
	P_{TG6} (MW)	30	100	100.0000	96.7985	99.9572
	P_{TG7} (MW)	123	410	343.9435	358.4092	316.1286
	V_1 (p.u.)	0.95	1.1	1.0493	1.0533	1.0470
	V_2 (p.u.)	0.95	1.1	1.0443	1.0456	1.0449
	V_3 (p.u.)	0.95	1.1	1.0441	1.0453	1.0457
	V_6 (p.u.)	0.95	1.1	1.0563	1.0462	1.0429
	V_8 (p.u.)	0.95	1.1	1.0575	1.0424	1.0480
	V_9 (p.u.)	0.95	1.1	1.0323	1.0277	1.0295
	V_{12} (p.u.)	0.95	1.1	1.0306	1.0437	1.0400
	T_{19} (p.u.)	0.90	1.10	0.9759	0.9864	1.0058
	T_{20} (p.u.)	0.90	1.10	1.1000	1.0354	1.0652
	T_{31} (p.u.)	0.90	1.10	0.9580	0.9952	1.0279
	T_{35} (p.u.)	0.90	1.10	1.0059	1.0155	0.9929
	T_{36} (p.u.)	0.90	1.10	0.9655	0.9359	0.9724
Variable	T_{37} (p.u.)	0.90	1.10	1.0472	1.0311	0.9682
	T_{41} (p.u.)	0.90	1.10	0.9860	0.9923	0.9732
	T_{46} (p.u.)	0.90	1.10	0.9485	0.9738	0.9507
	T_{54} (p.u.)	0.90	1.10	0.9260	0.9170	0.9249
	T_{58} (p.u.)	0.90	1.10	0.9922	0.9830	1.0198
	T_{59} (p.u.)	0.90	1.10	0.9731	0.9567	0.9621
	T_{65} (p.u.)	0.90	1.10	0.9746	0.9616	1.0190
	T_{66} (p.u.)	0.90	1.10	0.9430	0.9636	0.9000
	T_{71} (p.u.)	0.90	1.10	1.0269	0.9983	1.0310
	T_{73} (p.u.)	0.90	1.10	1.0412	1.0067	0.9675
	T_{76} (p.u.)	0.90	1.10	0.9000	1.0132	1.0535
	T_{80} (p.u.)	0.90	1.10	1.0484	1.0409	1.0417
	Q_{TG1} (MVAr)	−140	200	52.1131	61.7561	27.0031
	Q_{TG2} (MVAr)	−17	50	28.0585	20.3215	37.9586
	Q_{TG3} (MVAr)	−10	60	26.9675	41.2500	24.8212
	Q_{TG4} (MVAr)	−8	25	12.7597	4.6859	−2.4807
	Q_{TG5} (MVAr)	−140	200	52.3377	12.5234	50.0058
	Q_{TG6} (MVAr)	−3	9	5.2316	8.1439	6.4411
	Q_{TG7} (MVAr)	−150	155	54.2682	83.7349	97.1273
Objective	Emission (t/h)			1.2998	1.6073	1.0859
	Cost ($/h)			42,378.2574	41,829.5401	45,553.6603
Operation indicator	V_D (p.u.)			1.0859	1.1717	1.1377
	P_{loss} (MW)			14.3990	15.4453	16.5127

Table A2. Best solutions offered by CMODE in case 2.

Case 2		Min	Max	Best Comp	Best Cost	Best Emission
	P_{TG1} (MW)	0	575.88	185.1707	132.3190	235.7068
	P_{PV1} (MW)	0	100	100.0000	100.0000	99.7895
	P_{TG2} (MW)	42	140	80.9551	51.1500	140.0000
	P_{PV2} (MW)	0	100	100.0000	100.0000	100.0000
	P_{TG3} (MW)	165	550	360.4079	433.4232	289.8099
	P_{PV3} (MW)	0	100	100.0000	100.0000	100.0000
	P_{TG4} (MW)	123	410	339.1958	349.9696	304.2488
	V_1 (p.u.)	0.95	1.1	1.0166	1.0226	1.0109
	V_2 (p.u.)	0.95	1.1	1.0128	1.0190	1.0081
	V_3 (p.u.)	0.95	1.1	1.0240	1.0155	1.0214
	V_6 (p.u.)	0.95	1.1	1.0390	1.0365	1.0374
	V_8 (p.u.)	0.95	1.1	1.0472	1.0507	1.0555
	V_9 (p.u.)	0.95	1.1	1.0195	1.0220	1.0278
	V_{12} (p.u.)	0.95	1.1	1.0236	1.0277	1.0406
	T_{19} (p.u.)	0.90	1.1	1.0382	1.0077	0.9963
	T_{20} (p.u.)	0.90	1.1	0.9816	0.9998	1.0451
	T_{31} (p.u.)	0.90	1.1	1.0515	1.0510	0.9962
	T_{35} (p.u.)	0.90	1.1	1.0412	0.9847	1.0599
	T_{36} (p.u.)	0.90	1.1	0.9137	0.9595	0.9000
Variable	T_{37} (p.u.)	0.90	1.1	0.9975	0.9760	0.9929
	T_{41} (p.u.)	0.90	1.1	0.9784	0.9857	1.0127
	T_{46} (p.u.)	0.90	1.1	0.9733	0.9496	0.9693
	T_{54} (p.u.)	0.90	1.1	0.9114	0.9109	0.9005
	T_{58} (p.u.)	0.90	1.1	0.9608	0.9420	0.9773
	T_{59} (p.u.)	0.90	1.1	0.9623	0.9402	0.9293
	T_{65} (p.u.)	0.90	1.1	0.9550	0.9766	0.9586
	T_{66} (p.u.)	0.90	1.1	0.9648	0.9585	0.9395
	T_{71} (p.u.)	0.90	1.1	0.9644	0.9970	0.9782
	T_{73} (p.u.)	0.90	1.1	1.0470	0.9901	1.0281
	T_{76} (p.u.)	0.90	1.1	0.9827	0.9926	0.9920
	T_{80} (p.u.)	0.90	1.1	0.9893	0.9876	0.9844
	Q_{TG1} (MVAr)	−140	200	16.9478	36.1716	−12.7746
	Q_{PV1} (MVAr)	−17	50	20.7363	38.8423	22.0496
	Q_{TG2} (MVAr)	−10	60	38.8840	15.6417	16.3274
	Q_{PV2} (MVAr)	−8	25	3.9737	−3.1597	−6.3003
	Q_{TG3} (MVAr)	−140	200	60.3842	56.9724	79.0276
	Q_{PV3} (MVAr)	−3	9	4.0140	3.5384	5.4230
	Q_{TG4} (MVAr)	−150	155	90.3729	91.3263	147.6832
	Emission(t/h)			1.1546	1.5145	0.9719
	Cost ($/h)			31,510.9641	30,778.9688	34,763.0205
Objective	C_T ($/h)			30,251.7905	29,519.7952	33,504.8575
	C_V ($/h)			1259.1736	1259.1736	1258.1630
Operation	V_D (p.u.)			0.9721	0.9982	0.9315
indicator	P_{loss} (MW)			14.9295	16.0618	18.7548

References

1. Nanda, J.; Hari, L. Economic emission load dispatch with line flow constraints using a classical technique. *IEEE Proc.-Gener. Transm. Distrib.* **1994**, *141*, 1–10. [CrossRef]
2. Hargreaves, J.J.; Hobbs, B.F. Commitment and dispatch with uncertain wind generation by dynamic programming. *IEEE Trans. Sustain. Energy* **2012**, *3*, 724–734. [CrossRef]

3. Xiong, G.; Yuan, X.; Mohamed, A.; Chen, J.; Zhang, J. Improved binary gaining–sharing knowledge-based algorithm with mutation for fault section location in distribution networks. *J. Comput. Des. Eng.* **2022**, *9*, 393–405. [CrossRef]

4. Pulluri, H.; Naresh, R.; Sharma, V. An enhanced self-adaptive differential evolution based solution methodology for multiobjective optimal power flow. *Appl. Soft Comput.* **2017**, *54*, 229–245. [CrossRef]

5. El-Sattar, S.A.; Kamel, S.; Sehiemy, R.; Jurado, F.; Yu, J. Single- and multi-objective optimal power flow frameworks using Jaya optimization technique. *Neural Comput. Appl.* **2019**, *31*, 8787–8806. [CrossRef]

6. Chen, G.A.; Qian, J.; Zhang, Z.; Li, S. Application of modified pigeon-inspired optimization algorithm and constraint-objective sorting rule on multi-objective optimal power flow problem. *Appl. Soft Comput. J.* **2020**, *92*, 106321. [CrossRef]

7. Naderi, E.A.; Pourakbari-Kasmaei, M.; Cerna, F.; Lehtonen, M. A novel hybrid self-adaptive heuristic algorithm to handle single- and multiobjective optimal power flow problems. *Electr. Power Energy Syst.* **2021**, *125*, 106492. [CrossRef]

8. Reddy, S.S. Solution of multi-objective optimal power flow using efficient meta-heuristic algorithm. *Electr. Eng.* **2017**, *100*, 401–413. [CrossRef]

9. Abbasi, M.; Abbasi, E.; Mohammadi-Ivatloo, B. Single and multi-objective optimal power flow using a new differential-based harmony search algorithm. *J. Ambient Intell. Humaniz. Comput.* **2020**, *12*, 851–871. [CrossRef]

10. Biswas, P.; Suganthan, P.N.; Mallipeddi, R.; Amaratunga, G. Multi-objective optimal power flow solutions using a constraint handling technique of evolutionary algorithms. *Soft Comput.* **2020**, *24*, 2999–3023. [CrossRef]

11. Xiong, G.; Shuai, M.; Hu, X. Combined heat and power economic emission dispatch using improved bare-bone multi-objective particle swarm optimization. *Energy* **2022**, *244*, 123108. [CrossRef]

12. Warid, W.; Hizam, H.; Mariun, N.; Wahab, N. A novel quasi-oppositional modified Jaya algorithm for multi-objective optimal power flow solution. *Appl. Soft Comput.* **2018**, *65*, 360–373. [CrossRef]

13. Shi, B.; Yan, L.; Wu, W. Multi-objective optimization for combined heat and power economic dispatch with power transmission loss and emission. *Energy* **2013**, *56*, 135–143. [CrossRef]

14. Hua, Y.; Jin, Y.; Hao, K. A clustering-based adaptive evolutionary algorithm for multiobjective optimization with irregular Pareto fronts. *IEEE Trans. Cybern.* **2019**, *7*, 2758–2770. [CrossRef]

15. Li, R.; Gong, W.; Lu, C. A reinforcement learning based RMOEA/D for bi-objective fuzzy flexible job shop scheduling. *Expert Syst. Appl.* **2022**, *203*, 117380. [CrossRef]

16. Zhang, J.; Xiong, G.; Zou, X.; Yuan, X. Multi-objective economic-environmental dispatch considering wind power and small runoff hydropower. *Autom. Electr. Power Syst.* **2021**, *45*, 1–8.

17. Theocharides, S.; Theristis, M.; Makrides, G.; Kynigos, M.; Spanias, C.; Georghiou, G.E. Comparative Analysis of Machine Learning Models for Day-Ahead Photovoltaic Power Production Forecasting. *Energies* **2021**, *14*, 1081. [CrossRef]

18. Theocharides, S.; Makrides, G.; Livera, A.; Theristis, M.; Kaimakis, P.; Georghiou, G.E. Day-ahead photovoltaic power production forecasting methodology based on machine learning and statistical post-processing. *Appl. Energy* **2020**, *268*, 115023. [CrossRef]

19. Xiong, G.; Li, L.; Mohamed, A.W.; Yuan, X.; Zhang, J. A new method for parameter extraction of solar photovoltaic models using gaining–sharing knowledge based algorithm. *Energy Rep.* **2021**, *7*, 3286–3301. [CrossRef]

20. Talavera, D.L.; Muñoz-Cerón, E.; de la Casa, J.; Lozano-Arjona, D.; Theristis, M.; Pérez-Higueras, P.J. Complete Procedure for the Economic, Financial and Cost-Competitiveness of Photovoltaic Systems with Self-Consumption. *Energies* **2019**, *12*, 345. [CrossRef]

21. Jones, C.B.; Theristis, M.; Darbali-Zamora, R.; Ropp, M.E.; Reno, M.J.; Lave, M.S. Switch Location Identification for Integrating a Distant Photovoltaic Array Into a Microgrid. *IEEE Access* **2022**, *10*, 57902–57913. [CrossRef]

22. Shi, J.; Zhu, Q.; Li, J. A novel hierarchical clustering algorithm with merging strategy based on shared subordinates. *Appl. Intell. Int. J. Artif. Intell. Neural Netw. Complex Probl. Solving Technol.* **2022**, *52*, 8635–8650. [CrossRef]

23. Biswas, P.; Suganthan, P.N.; Mallipeddi, R.; Amaratunga, G. Optimal power flow solutions using differential evolution algorithm integrated with effective constraint handling techniques. *Eng. Appl. Artif. Intell.* **2018**, *68*, 81–100. [CrossRef]

24. Biswas, P.P.; Suganthan, P.N.; Qu, B.; Amaratunga, G.A. Multi-objective economic-environmental power dispatch with stochastic wind-solar-small hydro power. *Energy* **2018**, *150*, 1039–1057. [CrossRef]

25. Qu, B.; Liang, J.; Zhu, Y.; Suganthan, P.N. Solving dynamic economic emission dispatch problem considering wind power by multi-objective differential evolution with ensemble of selection method. *Nat. Comput.* **2017**, *18*, 695–703. [CrossRef]

26. Yu, X.; Yu, X.; Lu, Y.; Sheng, J. Economic and emission dispatch using ensemble multi-objective differential evolution algorithm. *Sustainability* **2018**, *10*, 418. [CrossRef]

27. Qiao, B.; Liu, J.; Hao, X. A multi-objective differential evolution algorithm and a constraint handling mechanism based on variables proportion for dynamic economic emission dispatch problems. *Appl. Soft Comput.* **2021**, *108*, 107419. [CrossRef]

28. Xiong, G.; Zhang, J.; Shi, D.; Zhu, L.; Yuan, X. Parameter extraction of solar photovoltaic models via quadratic interpolation learning differential evolution. *Sustain. Energy Fuels* **2020**, *4*, 5595–5608. [CrossRef]

29. Xu, R.; Wunsch, I. Survey of clustering algorithms. *IEEE Trans. Neural Netw.* **2005**, *16*, 645–678. [CrossRef]

30. Biswas, P.; Mallipeddi, R.; Arora, P.; Suganthan, P.N. Optimal placement and sizing of FACTS devices for optimal power flow in a wind power integrated electrical network. *Neural Comput. Appl.* **2021**, *33*, 6753–6774. [CrossRef]

31. Deb, K.; Agarwal, R.B. An evolutionary many-objective optimization algorithm using reference-point-based nondominated sorting approach, part I: Solving problems with box constraints. *IEEE Trans. Evol. Comput.* **2014**, *18*, 577–601. [CrossRef]

32. Edib, S.N.; Lin, Y.; Vokkarane, V.; Qiu, F.; Yao, R.; Zhao, D. Optimal PMU Restoration for Power System Observability Recovery after Massive Attacks. *IEEE Trans. Smart Grid* **2021**, *12*, 1565–1576. [CrossRef]

33. Coronel, E.; Baran, B.; Gardel, P. Optimal placement of remote controlled switches in electric power distribution systems with a Meta-heuristic Approach. *Lat. Am. Trans.* **2022**, *45*, 590–598. [CrossRef]
34. Deb, K.; Pratap, A.; Agarwal, S.; Meyarivan, T. A fast and elitist multi-objective genetic algorithm: NSGA-II. *IEEE Trans. Evol. Comput.* **2010**, *6*, 182–197. [CrossRef]
35. Yang, S.; Li, M.; Liu, X.; Zheng, J. A grid-based evolutionary algorithm for many-objective optimization. *IEEE Trans. Evol. Comput.* **2013**, *17*, 721–736. [CrossRef]